Investigations of the Mechanism of Gold Nanoparticle Stability and Surface Functionalization in Capillary Electrophoresis

Michael R. Ivanov, **Heidi R. Bednar**, and **Amanda J. Haes**[*]
University of Iowa, Department of Chemistry, Iowa City, Iowa 52242

Abstract

Covalently functionalized gold nanoparticles influence capillary electrophoresis separations of neurotransmitters in a concentration and surface chemistry–dependent manner. Gold nanoparticles with either primarily covalently functionalized carboxylic acid (Au@COOH) or amine (Au@NH$_2$) surface groups are characterized using extinction spectroscopy, transmission electron microscopy, and zeta potential measurements. The impact the presence of nanoparticles and their surface chemistry is investigated, and at least three nanoparticle-specific mechanisms are found to effect separations. First, the degree of nanoparticle-nanoparticle interactions is quantified using a new parameter termed the critical nanoparticle concentration (CNC). CNC is defined as the lowest concentration of nanoparticles that induces predominant nanoparticle aggregation under specific buffer conditions and is determined using dual-wavelength photodiode array detection. Once the CNC has been exceeded, reproducible separations are no longer observed. Second, nanoparticle-analyte interactions are dictated by electrostatic interactions which depend on the pK$_a$ of the analyte and surface charge of the nanoparticle. Finally, nanoparticle-capillary interactions occur in a surface chemistry dependent manner. Run buffer viscosity is influenced by the formation of a nanoparticle steady-state pseudo-stationary phase along the capillary wall. Despite differences in buffer viscosity leading to changes in neurotransmitter mobilities, no significant changes in electroosmotic flow were observed. As a result of these three nanoparticle-specific interactions, Au@NH$_2$ nanoparticles increase the mobility of the neurotransmitters while a smaller opposite effect is observed for Au@COOH nanoparticles. Understanding nanoparticle behavior in the presence of an electric field will have significant impacts in separation science where nanoparticles can serve to improve either the mobility or detection sensitivity of target molecules.

Keywords

Gold nanoparticles; nanoparticle functionalization; capillary electrophoresis; nanoparticle pseudo-stationary phase

Nanometer-sized particles exhibit unique chemical and physical properties which depend on their shape, size, and local environment. Nanoparticles have been combined with separation science to optimize detection,[1–8] facilitate separation of nanoparticles themselves,[9–11] and dramatically improve resolution of target molecules.[12–19] Furthermore, the use of nanoparticles have both stabilized separation efficiency and decreased electroosmotic flow.[9, 20, 21] The high surface energy of noble metal nanoparticles, however, can induce aggregation in the harsh buffer conditions required for optimized capillary electrophoresis separations.[22] Polymer additives[12–14] and nanoparticle surface chemistry[21, 23] have improved nanoparticle utility in separation science; however, there has been no systematic study that correlates the

CORRESPONDING AUTHOR FOOTNOTE. Phone: (319) 384-3695; Fax: (319) 335-1270; Email: E-mail: amanda-haes@uiowa.edu; University of Iowa, Department of Chemistry, 204 IATL, Iowa City, Iowa 52242.

concentration, stability, and surface chemistry of a nanoparticle with a fixed size and shape to analyte mobility in capillary electrophoresis. These studies have been limited because nanoparticle parameters are difficult to assess in the dynamic environment of a capillary in an electric field.

One method to understand the function of nanoparticles in a separation is by tracking the novel, size-dependent properties of the injected nanomaterials. For instance, gold nanoparticles exhibit a strong extinction (absorption + scattering) band that can be tuned throughout visible to near infrared wavelengths.[24] This extinction band results when the incident photon frequency is in resonance with the collective oscillation of the conduction band electrons and is known as the localized surface plasmon resonance (LSPR).[24] Large molar extinction coefficients ($\sim 3 \times 10^{11}$ M^{-1} cm^{-1})[25–27] are a result of the LSPR and can be used to calculate the concentration and size of nanoparticles in solution[28] as well as to assess nanoparticle aggregation.

To understand the optical properties of gold nanoparticles, it is important to consider not only their composition, shape, and size but also the local environment.[29] The local dielectric environment includes both solvent molecules as well as other nanoparticles. When the electromagnetic fields from two different nanoparticles interact, a complex LSPR is produced.[30] An important implication of nanoparticle aggregation is shifting of the LSPR to lower energies versus isolated nanoparticles.

Surface chemistry has been used to both prevent disorganized or induce organized aggregation of solution-phase nanoparticles.[31–34] In order to prevent uncontrolled aggregation, nanoparticle surfaces have been modified with capping molecules that form an electrostatically-induced steric barrier between nanoparticles.[35] Alternatively, to allow controlled nanoparticle aggregation in specific environmental conditions, capping molecules can be assembled onto the surface of the nanoparticles.

Herein, the surface chemistry on gold nanoparticles will be varied and allowed to interact with target molecules during capillary electrophoresis. The nanoparticle pseudo-stationary phase will comprise only 2% of the total capillary volume which has been optimized so the optical properties of the nanoparticles can be easily monitored. The resulting stability of the nanoparticles will be assessed using dual-wavelength photodiode array (PDA) detection. The mobility of three neurotransmitters will be evaluated in the presence of both positively and negatively charged covalently stabilized gold nanoparticles as well as size-matched silica and citrate reduced gold nanoparticles. For covalently functionalized nanoparticles, the effective surface charge impacts the mobility of the neurotransmitters in a concentration-dependent manner. Positively charged gold nanoparticles will be shown to be more stable and interact more strongly with both the analytes and capillary wall than the negatively charged nanoparticles in the presence of an electric field. In all cases, the formation of nanoparticle aggregates decreases the migration times of the targeted molecules. We expect that as the nanoparticle pseudo-stationary phase volume increases, the magnitude of these responses will also increase and therefore be more efficiently implemented in the separation of target chemical and biological species.

RESULTS AND DISCUSSION

Bulk Optical and Charge Characterization of Gold Nanoparticles

The LSPR of gold nanoparticles[36] has been exploited to assess the degree of nanoparticle stability as a function of surface chemistry and local environment. As shown from TEM data in Figure 1A, citrate reduced gold nanoparticles (Au@citrate) have an average diameter of 13.3 ± 0.6 nm. Zeta potential measurements reveal the nanoparticles are highly stable and have

an average surface charge of -39.7 ± 0.7 mV at pH 9.3. Evaluation of the optical properties of the nanoparticles supports the stability indicated by the zeta potential measurements. The extinction data clearly demonstrate the stability of Au@citrate nanoparticles in both water and buffer (Figure 1A-1 and 1A-2).

Despite the high degree of stability in bulk solution, Au@citrate nanoparticles are unstable inside a capillary.[2, 15] As a result, the electrostatically-attached citrate molecules have been replaced by a more stable and covalently-bound surface functionalization.[21, 37] First, the citrate on the gold nanoparticle surface is replaced by thioctic acid. This step improves nanoparticle stability and reduces uncontrolled aggregation which typically occurs in direct exchange reactions. Subsequently, a portion of the easily displaced thioctic acid group is replaced by 6-mercaptohexanoic acid for Au@COOH nanoparticles or 6-aminohexanethiol for Au@NH_2 nanoparticles (Scheme 1). Each exchange results in a nanoparticle type composed of a mixed monolayer with distinct surface chemistries.

As shown in Figure 1B, Au@COOH nanoparticles exhibit an extinction maximum that is centered at ~522 nm in both water and buffer. In both solution environments, a slight shoulder is observed at ~615 nm and is characteristic of reduced interparticle interactions and electromagnetic coupling between nanoparticles. In comparison to Au@citrate nanoparticles, Au@COOH nanoparticles are slightly smaller (average diameter = 10.9 ± 1.8 nm) and exhibit a zeta potential that is slightly less negative (-36.4 ± 2.0 mV at pH 9.3). This small change in nanoparticle diameter is likely an artifact of nanoparticle purification required in the ligand exchange reactions. For carboxylic acid terminated monolayers, the surface pK_a ranges from 5 to 8 versus 4 to 5 in solution.[38–40]

Representative extinction spectra and a TEM image for Au@NH_2 nanoparticles are shown in Figure 1C. In contrast to both Au@citrate and Au@COOH nanoparticles, Au@NH_2 nanoparticles exhibit a large degree of instability in buffer (pH 9.3) which is supported by an average zeta potential equal to 5.9 ± 0.2 mV at pH 9.3. It should be noted that as the zeta potential approaches zero, inherent nanoparticle stability worsens. Importantly, the surface pK_a for amine terminated nanoparticles ranges from 4 to 6 or ~2 – 4 units lower than the solution pK_a values.[41–43]

Clearly, surface pK_a values are important for the ultimate stability of nanoparticles in solution. At pH 9.3, the amine groups will be more protonated with an overall positive surface charge, a result supported by positive zeta potential measurements for Au@NH_2 nanoparticles. It should be noted that for these nanoparticles, the effective surface charge arises from both the exchanged amine molecules (6-amino-hexanthiol) and the remaining un-exchanged molecules (thioctic acid) yielding ~65–70% amine group surface coverage (estimated from zeta potential measurements).

Evaluation of Gold Nanoparticle Stability in a Capillary

It is important to identify whether solution phase nanoparticle clusters have formed reversibly (flocculated) or irreversibly (aggregated). As shown in Figure 1, if the majority of the nanoparticles are in their isolated form, the nanoparticles will absorb strongly at 520 nm and weakly at 600 nm. By taking the ratio of the absorbance (R) at both wavelengths as follows:

$$R = \frac{\text{Absorbance}_{520}}{\text{Absorbance}_{600}}$$

(1)

where Absorbance$_{520}$ = absorbance collected at 520 nm and Absorbance$_{600}$ = absorbance collected at 600 nm, nanoparticle stability can be quantified. For highly stable or isolated gold

nanoparticles (i.e. Figure 1C-1), R is ~ 3.5 – 4. When nanoparticles electromagnetically couple, the ratio decreases and will eventually approach 0.

The large magnitude of the nanoparticle extinction cross section permits the detection of nanoparticles down to ~600 pM in a capillary (S/N ~ 4+). While photodiode array (PDA) detector sensitivity is poor (versus UV-detection) and the extinction cross sections for isolated and aggregates vary with size/degree of nanoparticle interactions, the combination of capillary electrophoresis with multi-wavelength PDA detection provides for the separation and detection of aggregates from isolated nanoparticles.

As shown in Figure 2A-i, when a 2% total volume plug length of 1.5 nM Au@COOH is injected into a capillary, a band with a migration time = 6.1 minutes is observed in the electropherograms collected at both 520 and 600 nm. Using Equation 1, the ratio between these band areas is ~3.8 ± 0.3. This band has a shoulder centered at ~6.4 minutes which has an R value of 2.9 ± 0.7. To improve the characterization of nanoparticles both outside and inside the capillary, we have defined a new attribute called the "critical nanoparticle concentration" (CNC). The CNC, a parameter similar to the critical micelle concentration in micellar electrokinetic chromatography (MEKC), is the lowest concentration of nanoparticles that induces dominant nanoparticle aggregation (versus stable nanoparticles) under specific buffer conditions. Experimentally the CNC is defined by a value of ratio band areas (Equation 1) at 50% of the total value for isolated nanoparticles.

When Au@COOH nanoparticle concentration is increased to 2.5 nM, three notable differences are observed in the resulting electropherograms (Figure 2A-ii) versus the lower nanoparticle concentration (Figure 2A-i). First, as expected, the intensities of the nanoparticle bands at both 520 and 600 nm increase. Second, two (unresolved) bands with migration times centered at 6.1 (shoulder) and 6.4 minutes (primary band) are detected at the two wavelengths. This indicates multiple nanoparticle species are being detected. Finally, the band shape in Figure 2A-ii (600 nm) is significantly broader than Figure 2A-ii, characteristic of a distribution of aggregate sizes.

Determination of the CNC for Au@COOH nanoparticles is shown in Figure 2B. As nanoparticle concentration increases, the area for the band centered at 6.1 minutes (band 1) decreases slightly while an increase in the area for a second band that is centered at 6.4 minutes (band 2) is observed. Using Equation 1, band 1 maintains R values ~ 3.8; characteristic of isolated nanoparticles. As nanoparticle concentration increases, band 2 area decreases from 2.9 ± 0.7 (at 1.5 nM) to 0.8 ± 0.6 (at 3.0 nM). As a result, band 2 is attributed to nanoparticle aggregates. From these data, the CNC is calculated at ~1.8 nM.

When Au@NH$_2$ nanoparticles are injected into the capillary; surface chemistry-dependent migration times are observed. At all concentrations studied, bands centered at 3.3 and 4.4 minutes are detected at 520 and 600 nm. Using Equation 1, for 1.5 nM Au@NH$_2$ (Figure 2C-i), R = 3.9 ± 0.2 for band 1 and agrees with the extinction intensity ratio. This result indicates nanoparticles are behaving as isolated instead of aggregated/flocculated nanoparticles as their characterization outside the capillary suggests. The ratio for band 2 is 2.3 ± 0.7 indicative of nanoparticle aggregation.

At higher concentrations of Au@NH$_2$ nanoparticles (3.5 nM), PDA measurements reveal similar band shapes at 520 and 600 nm (Figure 2C-ii). Band 1 displays a migration time of ~ 3.3 minutes and a ratio = 3.9 ± 0.2 while maintaining similar shapes at both wavelengths. Band 2, however, has obvious differences in both relative absorbance area and shape versus lower nanoparticle concentrations. Notably, band shape is highly dependent on detection wavelength. For example in Figure 2C-i, band 2 is significantly broader at 600 nm versus 520 nm indicating detection of a heterogeneous distribution of nanoparticle aggregates.

The CNC for Au@NH$_2$ nanoparticles is determined in Figure 2D. Similar to Au@COOH nanoparticles, Au@NH$_2$ nanoparticles reveal concentration dependent trends in the ratio data for both bands 1 and 2. For all concentrations studied, band 1 maintains a ratio for ~ 3.9 indicative of isolated nanoparticles. The ratio of band 2, however, decreases with increasing concentration. Here, the CNC is estimated at 2.3 nM, a result surprising given the instability of these nanoparticles outside the capillary.

Clearly, differences in nanoparticle surface chemistries are observed. Despite injections of equal concentrations, the Au@NH$_2$ nanoparticles exhibit ~one-half the overall PDA-collected absorbance intensity versus Au@COOH nanoparticles. This could indicate three different phenomena. Au@NH$_2$ nanoparticles are more likely to (1) interact with the capillary wall, (2) diffuse through the capillary below the detection limit of the PDA detector, and/or (3) exhibit injection problems versus Au@COOH nanoparticles. Dark-field microcopy reveals that the nanoparticles are not visibly attached to the capillary walls (data not shown). Similar current changes (in amperes) are observed when the nanoparticle plug exits the capillary suggesting that the Au@NH$_2$ nanoparticles more freely diffuse along the capillary wall than the Au@COOH nanoparticles thereby resulting in lower signal strengths.

Impact of Nanoparticle Functionality and CNC on the Separation of Neurotransmitters

To investigate the impact nanoparticles have on analyte mobility, as before, a 2% plug of the total capillary volume of Au@COOH and Au@NH$_2$ nanoparticles as well as size-matched silica and Au@citrate nanoparticle controls were injected into a capillary at various concentrations prior to a plug of three neurotransmitters (dopamine, epinephrine, and pyrocatechol). The nanoparticles travel more slowly than the neurotransmitters thereby serving as a mobile pseudo-stationary phase. In all cases, the elution order of the neurotransmitters is (d) dopamine, (e) epinephrine, and (p) pyrocatechol (Supplementary Information).

Trends in these data are clearer when the migration of only one neurotransmitter is analyzed. In Figure 3, the migration time of the pyrocatechol band remains statistically constant upon the addition of either silica or Au@citrate nanoparticles (Figure 3A and 3B, respectively). Upon increasing the concentration of Au@COOH nanoparticles, the migration time of pyrocatechol increases until its CNC is exceeded (Figure 3C). Upon achieving the CNC, uncontrolled aggregation occurs and the capillary clogs. In contrast, as Au@NH$_2$ nanoparticle concentration increases, pyrocatechol migration times decrease (Figure 3D). This is the first demonstration of increasing analyte mobility with gold nanoparticles! It should be noted that these trends are similar for each neurotransmitter used in this study.

We hypothesize at least three mechanisms are influencing this separation. First, Au@NH$_2$ nanoparticles have a higher CNC than the other nanoparticles studied, and this improved stability in the capillary leads to more reproducible separations. This likely arises because Au@NH$_2$ nanoparticles form a mobile viscous layer at the capillary surface. Second, the effective "positive" surface charge on the Au@NH$_2$ nanoparticles are more strongly attracted to the negative anode, the capillary wall, and negatively charged/neutral neurotransmitters. As a result of these attractions, increased electroosmotic flow and a larger influence on analyte mobility are measured for Au@NH$_2$ versus the other functionalized nanoparticles studied. Finally, the positively charged Au@NH$_2$ nanoparticles are more strongly attracted to the capillary wall than the other nanoparticles studied. While the nanoparticles do not bind irreversibly to the capillary wall, a dilution effect is likely occurring as observed with the PDA measurements.

Finally, Figure 4 shows how nanoparticle concentration and functionalization impacts the mobility of dopamine. Au@COOH nanoparticles have a slight retarding effect while Au@NH$_2$ nanoparticles clearly increase the migration time of the same molecule. Closer

examination of these mobility changes reveal that while the negatively charged Au@COOH nanoparticles systematically decrease the analyte mobility, the changes in mobility are not significantly different among the various nanoparticle concentrations studied. When Au@NH$_2$ nanoparticles are included in the separation, the neurotransmitter mobility significantly increases as determined from 95% confidence interval and T-test analyses.

Evaluation of Mobility Variations of Neurotransmitters in the Presence of Covalently-Functionalized Nanoparticles

In these studies, it is important to consider how the inherent mobility of the molecules has changed with both (1) variations in Au@NH$_2$ nanoparticle concentration as well as (2) versus Au@COOH nanoparticles. When nanoparticles are included in a separation, the electrophoretic mobility of a charged molecule may change and can be approximated using the Debye-Hückel-Henry theory:

$$\mu = \frac{q}{6\pi\eta r}$$

(2)

where q is the charge on the species, η is the viscosity of the surrounding buffer, and r is the radius of the species.[44] Because no significant effect on electroosmotic flow was observed in the presence of nanoparticles, either the charge of the molecule, the size of the molecule, or the viscosity of the buffer must change if the electrophoretic mobility of the molecule varies. The effective charge and size of the neurotransmitters remain constant regardless of nanoparticle inclusion. Consequently, buffer viscosity must increase if an increase in the electrophoretic mobility of the molecules is observed. Rearrangement of Equation 2 yields an approximation of the viscosity of the separation buffer. Assuming all molecular (dopamine) parameters are constant among injections, buffer viscosity increases by ~0.68% for 1.18 nM Au@COOH nanoparticles while a ~1.70% decrease is observed when 1.18 nM Au@NH$_2$ nanoparticles are included (versus control experiments).

Similar to a dynamic coating,[44] nanoparticles must reach a steady-state interaction with both molecules and the capillary wall. As observed in Figure 4A, below the CNC, the error in the mobility of dopamine decreases with increasing Au@COOH nanoparticle concentration. We hypothesize that because these negatively charged nanoparticles are weakly attracted to the capillary wall, the relaxation period does not reach steady-state and results in large deviations in observed analyte mobility. As the nanoparticle concentration increases, a steady-state environment[45] is achieved more efficiently, and the separation becomes systematically more reproducible until aggregation dominates.

The positively charged Au@NH$_2$ nanoparticles, on the other hand, are more strongly attracted to the capillary wall and achieve a steady-state much more quickly than the negatively charged Au@COOH nanoparticles. As observed in Figure 4B, when 0.22 nM Au@NH$_2$ nanoparticles are included, the mobility of dopamine is highly irreproducible; however, the reproducibility of the separation is greatly improved when the nanoparticle concentration exceeds ~0.5 nM but is less than the CNC. The readily formed nanoparticle containing viscous layer at the capillary wall will increase the mobility of the molecules as observed in Figure 4B.

Importantly, the nanoparticle pseudo-stationary phase used in these studies occupies less than 2% of the total capillary volume. Just as the viscous nanoparticle layer near the capillary is formed because of the dynamic nature of the system, it will also be destabilized. As the length of the nanoparticle pseudo-stationary phase increases, impacts on analyte mobility will likely increase, also. Furthermore, these results will likely be magnified as nanoparticle concentration and/or plug length are increased.[12–14]

CONCLUSIONS

In summary, the optical properties of covalently functionalized gold nanoparticles have been used to investigate the stability of the nanoparticles as well as the mobilities of dopamine, epinephrine and pyrocatechol in capillary electrophoresis. The nanoparticle pseudo-stationary phase comprised only 2% of the total capillary volume allowing the optical properties of aggregated and isolated nanoparticles to be easily distinguished. The stability of both amine and carboxylated gold nanoparticles was determined using extinction spectroscopy and zeta potential measurements outside the capillary. Inside the capillary, the lowest nanoparticle concentration which induced aggregation (i.e. CNC) was subsequently evaluated using dual wavelength PDA detection.

These findings demonstrate that effective surface charge impacts interactions of nanoparticles with analytes, the capillary wall, and other nanoparticles. These interactions directly influence the mobility of the nanoparticles. Furthermore, the mobility of the neurotransmitters increases in the presence of amine terminated nanoparticles but decreases slightly with carboxyl terminated nanoparticles. Below the CNC, this observation is dominated by the formation of a mobile pseudo-stationary phase at the capillary wall which is hypothesized to increase the local buffer viscosity. The presented approach of exploiting nanoparticle behavior in the presence of an electric field will have significant impacts in separation science where nanoparticles are employed. Further investigations will lead to more controlled improvements in the separation and detection of target biological and chemical species.

METHODS

Reagents and Chemicals

All chemicals were purchased from Sigma-Aldrich (St Louis, MO) unless otherwise noted. 6-Amino-hexanethiol was purchased from Dojindo Chemicals (Gaithersburg, MD). Silica nanoparticles (diameter, $d = 15$ nm) were purchased from Nanostructures and Amorphous Materials (Los Alamos, NM). Water was purified to a resistivity greater than 18 MΩ cm^{-1} using a Barnstead Nanopure (Dubuque, IA) water filtration system. Solutions were filtered through 13 mm diameter, 0.45 µm nylon filters from Whatman (Middlesex, UK) prior to use.

Fused silica capillary was purchased from Polymicro (Phoenix, AZ) and had an internal diameter of 75 µm, an outer diameter of 360 µm, and an external polyimide coating. The total capillary length was 60.2 cm with a 50 cm effective length.

Nanoparticle Synthesis

Prior to synthesis, all glassware were cleaned with aqua regia. Gold nanoparticles were prepared using an established procedure.[36] Briefly, 20 mg of $HAuCl_4$ was dissolved in 50 mL water and brought to a rolling boil while stirring using a reflux condenser. Trisodium citrate (60 mg) was dissolved in water (5 mL) and added to the boiling solution. Initially, the solution turned very dark violet and quickly changed to red. The solution was refluxed for an additional 15–20 minutes. After cooling, the resulting nanoparticle solution was stored in a brown bottle until use. A standard estimation model was used to calculate the concentration of gold nanoparticles.[28] This was achieved and validated in a multi-step process. First, the average nanoparticle diameter was obtained from TEM measurements. Based on this value, a corresponding molar extinction coefficient (ε) was calculated from the standard estimation model. Next, the nanoparticle concentration was verified using the extinction intensity at 450 nm versus its extinction maximum. For Au@citrate nanoparticles, this concentration was evaluated as 7.82 nM.

Nanoparticle Functionalization and Preparation

Functionalized nanoparticles were synthesized by modifying a multi-step procedure.[37] First, citrate molecules on the nanoparticle surface were displaced by thioctic acid. To do this, 0.4 mL of thioctic acid (in ethanol, 10 mM or 4 mM for the carboxylated and amine functionalization, respectively) was added to the previously synthesized citratereduced gold nanoparticles in a ratio of 0.1 mL thioctic acid to 1 mL nanoparticles. This solution was stirred overnight so that the reaction could reach equilibrium. The nanoparticles were then centrifuged at 15,000 rpm for 20 min, and the supernatant was discarded. The resulting nanoparticles were resuspended in water to a concentration of 7.82 nM.

Au@COOH nanoparticles were functionalized with 6-mercaptohexanoic acid by first adjusting the pH of the thioctic acid-modified nanoparticle solution to 11 with 1 M NaOH. Next, an ethanolic solution of 10 mM 6-mercaptohexanoic acid was added to the nanoparticle solution in a ratio of 0.1 mL 6-mercaptohexanoic acid to 1 mL nanoparticles and stirred overnight in an ice bath. The resulting carboxylic acid terminated nanoparticles were centrifuged at 15,000 rpm for 20 minutes, the supernatant discarded, and the nanoparticles resuspended in water pH adjusted with 1 M NaOH to a concentration of 1.74 nM prior to use.

Au@NH$_2$ nanoparticles were functionalized using a similar procedure. In an ice bath, 4 mM 6-amino-1-hexanethiol (in ethanol) was added to thioctic-acid stabilized nanoparticles without adjustment of solution pH (in a ratio of 0.1 mL 6-amino-hexanethiol to 1 mL nanoparticles). Within five minutes, the color of the nanoparticle solution turned from burgundy to purple. After one hour, 1 M HCl (0.1mL 1 M HCl to 1 mL nanoparticles) was added and the nanoparticle solution immediately changed to a burgundy color. This solution was stirred over night in an ice bath. Next, the resulting solution was centrifuged at 15,000 rpm for 20 minutes, the supernatant discarded, and the nanoparticles resuspended in water pH adjusted with 1 M HCl to a (nanoparticle) concentration of 1.31 nM prior to use.

Varying nanoparticle concentrations were obtained by either diluting the nanoparticles in separation buffer or by preconcentrating the nanoparticles via centrifugation (15,000 rpm for 20 minutes) and resuspending them in buffer.

Silica nanoparticles were suspended in water to a stock concentration of 7.82 nM and diluted to the desired concentration in separation buffer.

Buffer Preparation

50 mM tetraborate buffer (pH 9.3) was prepared using boric acid and sodium tetraborate. The pH was adjusted with 1 M NaOH. The separation buffer was prepared by diluting this stock solution to a concentration of 10 mM tetraborate. All buffers were filtered prior to use.

Sample Preparation

Three neurotransmitters (dopamine, epinephrine, and pyrocatechol) were used in these studies. Stock solutions (5 mM) of each were made in 10 mM tetraborate buffer. These samples were diluted to a final concentration of 50 µM in the same buffer and filtered prior to use.

Capillary Conditioning

The capillary was conditioned prior to each run as follows. First, the capillary was rinsed with 0.1 M HNO$_3$ (20 psi for 5 min), water (20 psi for 2.25 min), 1 M NaOH (20 psi for 2.25 min), water (20 psi for 2.25 min), and 50 mM sodium tetraborate buffer (20 psi for 2.25 min). The capillary was then filled with the separation buffer (20 psi for 3 min) prior to each separation.

Capillary Electrophoresis Equipment

All separations were performed on a Beckman Coulter PACE-MDQ capillary electrophoresis instrument equipped with a UV detector, photodiode array (PDA) detector, and capillary cooling. Capillary temperature was maintained at 25° C. UV detection occurred at 214 nm, and PDA detection occurred at both 520 nm and 600 nm. The instrument was utilized per manufacturer recommendations.

The neurotransmitter sample and nanoparticle solution were injected sequentially into the capillary to reduce possible nanoparticle instability caused by the molecules. The injection scheme for these materials was as follows: 5 sec (1 psi) nanoparticles, 1 sec (1 kV) buffer, and 10 sec (10 kV, normal polarity) neurotransmitters. The buffer plug helped to minimize cross-contamination between the sample vials. Separations were performed by applying a voltage of 20 kV (normal polarity) across the capillary.

Each experiment was performed in triplicate. While these effects were minimized, separations were performed in increasing nanoparticle concentration to reduce complications that might arise from nanoparticles that could remain in the capillary between runs. Data were analyzed using OriginPro 7.5 and Grams AI 7.0. Data shown in electropherograms have been normalized to account for slight variations in buffer and sample matrix. Normalization was performed by adjusting the migration time of epinephrine from the first run of the day to its average migration time for a series of control experiments in the absence of nanoparticles. The same adjustment factor was subsequently applied to all data from that day. The PDA data have been smoothed using a first order Savitzky-Golay fit (20 point window).

UV-Visible (UV-Vis) Spectroscopy

The optical properties and the overall stability of the gold nanoparticle solutions were evaluated in water and buffer using UV-Vis spectroscopy (USB4000, Ocean Optics, Dunedin, FL).

Zeta Potential

The effective surface charges on the gold nanoparticles were measured using zeta-potential (Malvern Instruments Zetasizer, Worcestershire, UK). Reported zeta potential measurements were collected in separation buffer at 1.96 nM Au@citrate, 1.96 nM silica, 1.77 nM Au@COOH, and 0.65 nM Au@NH$_2$ concentrations. Data were obtained using a monomodal acquisition and fit according to the Smoluchowski theory.

Transmission Electron Microscopy (TEM)

Homogeneity of the nanoparticles was characterized using TEM (JEOL JEM-1230). In all cases, ~2 µL of diluted nanoparticle solution (50% mixture in ethanol) was applied to a carbon-formvar coated copper grid (400 mesh, Ted Pella, Redding, CA) and allowed to air dry. Any remaining solution was removed with filter paper prior to TEM analysis.

Supplementary Material

Refer to Web version on PubMed Central for supplementary material.

ACKNOWLEDGMENT

REFERENCES

1. Shiddiky MJA, Shim Y-B. Trace Analysis of DNA: Preconcentration, Separation, and Electrochemical Detection in Microchip Electrophoresis Using Au Nanoparticles. Anal. Chem 2007;79:3724–3733. [PubMed: 17428034]

2. Pumera M, Wang J, Grushka E, Polsky R. Gold Nanoparticle-Enhanced Microchip Capillary Electrophoresis. Anal. Chem 2001;73:5625–5628. [PubMed: 11816598]

3. He L, Natan MJ, Keating CD. Surface-Enhanced Raman Scattering: A Structure-Specific Detection Method for Capillary Electrophoresis. Anal. Chem 2000;72:5348–5355. [PubMed: 11080886]

4. Connatser RM, Riddle LA, Sepaniak MJ. Metal-Polymer Nanocomposites for Integrated Microfluidic Separations and Surface Enhanced Raman Spectroscopic Detection. J. Sep. Sci 2004;27:1545–1550. [PubMed: 15638165]

5. Dijkstra RJ, Ariese F, Gooijer C, Brinkman UA. Raman Spectroscopy as a Detection Method for Liquid-Separation Techniques. Trends Anal. Chem 2005;24:304–323.

6. Dijkstra RJ, Gerssen A, Efremov EV, Ariese F, Brinkman UAT, Gooijer C. Substrates for the at-Line Coupling of Capillary Electrophoresis and Surface-Enhanced Raman Spectroscopy. Anal. Chim. Acta 2004;508:127–134.

7. Seifar RM, Dijkstra RJ, Gerssen A, Ariese F, Brinkman UAT, Gooijer C. At-Line Coupling of Capillary Electrophoresis and Surface-Enhanced Resonance Raman Spectroscopy. J. Sep. Sci 2002;25:814–818.

8. Nirode WF, Devault GL, Sepaniak MJ, Cole RO. On-Column Surface-Enhanced Raman Spectroscopy Detection in Capillary Electrophoresis Using Running Buffers Containing Silver Colloidal Solutions. Anal. Chem 2000;72:1866–1871. [PubMed: 10784155]

9. Wang Y, Ouyang J, Baeyens WRG, Delanghe JR. Use of Nanomaterials in Capillary and Microchip Electrophoresis. Exp. Rev. Prot 2007;4:287–298.

10. Liu F-K, Tsai M-H, Hsu Y-C, Chu T-C. Analytical Separation of Au/Ag Core/Shell Nanoparticles by Capillary Electrophoresis. J. Chrom. A 2006;1133:340–346.

11. Song X, Li L, Qian H, Fang N, Ren J. Highly Efficient Size Separation of Cdte Quantum Dots by Capillary Gel Electrophoresis Using Polymer Solution as Sieving Medium. Electrophoresis 2006;27:1341–1346. [PubMed: 16502461]

12. Tseng W-L, Huang M-F, Huang Y-F, Chang H-T. Nanoparticle-Filled Capillary Electrophoresis for the Separation of Long DNA Molecules in the Presence of Hydrodynamic and Electrokinetic Forces. Electrophoresis 2005;26:3069–3075. [PubMed: 16041701]

13. Lin Y-W, Huang M-F, Chang H-T. Nanomaterials and Chip-Based Nanostructures for Capillary Electrophoretic Separations of DNA. Electrophoresis 2005;26:320–330. [PubMed: 15657878]

14. Huang M-F, Kuo Y-C, Huang C-C, Chang H-T. Separation of Long Double-Stranded DNA by Nanoparticle-Filled Capillary Electrophoresis. Anal. Chem 2004;76:192–196. [PubMed: 14697050]

15. Neiman B, Grushka E, Lev O. Use of Gold Nanoparticles to Enhance Capillary Electrophoresis. Anal. Chem 2001;73:5220–5227. [PubMed: 11721922]

16. Neiman B, Grushka E, Gun J, Lev O. Organically Modified Silica Sol-Mediated Capillary Electrophoresis. Anal. Chem 2002;74:3484–3491. [PubMed: 12139058]

17. Nilsson C, Birnbaum S, Nilsson S. Use of Nanoparticles in Capillary and Microchip Electrochromatography. J. Chrom. A 2007;1168:212–224.

18. Nilsson C, Viberg P, Spegel P, Jornten-Karlsson M, Petersson P, Nilsson S. Nanoparticle-Based Continuous Full Filling Capillary Electrochromatography/Electrospray Ionization-Mass Spectrometry for Separation of Neutral Compounds. Anal. Chem 2006;78:6088–6095. [PubMed: 16944888]

19. Bächmann K, Göttlicher B. New Particles as Pseudostationary Phase for Electrokinetic Chromatography. Chromatogr 1997;45:249–254.

20. Liu F-K, Hsu Y-T, Wu C-H. Open Tubular Capillary Electrochromatography Using Capillaries Coated with Films of Alkanethiol-Self-Assembled Gold Nanoparticle Layers. J. Chrom. A 2005;1083:205–214.

21. Yu C-J, Su C-L, Tseng W-L. Separation of Acidic and Basic Proteins by Nanoparticle-Filled Capillary Electrophoresis. Anal. Chem 2006;78:8004–8010. [PubMed: 17134133]

22. Cao, G. Nanostructures and Nanomaterials: Synthesis, Properties and Applications. London: Imperial College Press; 2004.

23. Yang L, Guihen E, Holmes JD, Loughran M, O'Sullivan GP, Glennon JD. Gold Nanoparticle-Modified Etched Capillaries for Open-Tubular Capillary Electrochromatography. Anal. Chem 2005;77:1840–1846. [PubMed: 15762594]

24. Haes AJ, Haynes CL, McFarland AD, Schatz GC, Van Duyne RP, Zou S. Plasmonic Materials for Surface-Enhanced Sensing and Spectroscopy. MRS Bulletin 2005;30:368–375.

25. Jensen TR, Malinsky MD, Haynes CL, Van Duyne RP. Nanosphere Lithography: Tunable Localized Surface Plasmon Resonance Spectra of Silver Nanoparticles. J. Phys. Chem. B 2000;104:10549–10556.

26. Link S, El-Sayed MA. Spectral Properties and Relaxation Dynamics of Surface Plasmon Electronic Oscillations in Gold and Silver Nano-Dots and Nano-Rods. J. Phys. Chem. B 1999;103:8410–8426.

27. El-Sayed MA. Some Interesting Properties of Metals Confined in Time and Nanometer Space of Different Shapes. Acc. Chem. Res 2001;34:257–264. [PubMed: 11308299]

28. Haiss W, Thanh NTK, Aveyard J, Fernig DG. Determination of Size and Concentration of Gold Nanoparticles from Uv-Vis Spectra. Anal. Chem 2007;79:4215–4221. [PubMed: 17458937]

29. Kreibig, U.; Vollmer, M. Cluster Materials. Heidelberg, Germany: Springer-Verlag; 1995. p. 532

30. Ghosh S, Pal T. Interparticle Coupling Effect on the Surface Plasmon Resonance of Gold Nanoparticles: From Theory to Applications. Chemical Reviews 2007;107:4797–4862. [PubMed: 17999554]

31. Liz-Marzan LM. Tailoring Surface Plasmons through the Morphology and Assembly of Metal Nanoparticles. Langmuir 2006;22:32–41. [PubMed: 16378396]

32. Heath JR, Knobler CM, Leff DV. Pressure/Temperature Phase Diagrams and Superlattices of Organically Functionalized Metal Nanocrystal Monolayers: The Influence of Particle Size, Size Distribution, and Surface Passivant. J. Phys. Chem. B 1997;101:189–197.

33. Leff DV, Brandt L, Heath JR. Synthesis and Characterization of Hydrophobic, Organically Soluble Gold Nanocrystals Functionalized with Primary Amines. Langmuir 1996;12:4723–4730.

34. Rouhana LL, Jaber JA, Schlenoff JB. Aggregation-Resistant Water-Soluble Gold Nanoparticles. Langmuir 2007;23:12799–12801. [PubMed: 18004894]

35. Hunter, RJ. Introduction to Modern Colloid Science. Oxford University Press; 1993. p. 344

36. Grabar KC, Freeman RG, Hommer MB, Natan MJ. Preparation and Characterization of Au Colloid Monolayers. Anal. Chem 1995;67:735–743.

37. Lin S-Y, Tsai Y-T, Chen C-C, Lin C-M, Chen C. Two-Step Functionalization of Netural and Positively Charged Thiols onto Citrate-Stabilized Au Nanoparticles. J. Phys. Chem. B 2004;108:2134–2139.

38. Hu K, Bard A. Use of Atomic Force Microscopy for the Study of Surface Acid-Base Properties of Carboxylic Acid-Terminated Self-Assembled Monolayers. Langmuir 1997;13:5114–5119.

39. Creager SE, Clarke J. Contact-Angle Titrations of Mixed-Mercaptoalkanoic Acid/Alkanethiol Monolayers on Gold. Reactive Vs. Nonreactive Spreading, and Chain Length Effects of Surface Pka Values. Langmuir 1994;10:3675–3683.

40. van der Vegte EW, Hadziioannou G. Acid-Base Properties and the Chemical Imaging of Surface-Bound Functional Groups Studied with Scanning Force Microscopy. J. Phys. Chem. B 1997;101:9563–9569.

41. Nishiyama K, Kubo A, Ueda A, Taniguchi I. Surface Pka of Amine-Terminated Self-Assembled Monolayers Evaluted by Direct Observation of Counter Anion by Ft-Surface Enhanced Raman Spectroscopy. Chemistry Letters 2002:80–81.

42. Nitzan B, Margel S. Surface Modification.Ii. Functionalized of Solid Surfaces with Vinylic Monomers. Journal of Polymer Science, Part A: Polymer Chemistry 1997;35:171–181.

43. Mengistu TZ, Goel V, Horton JH, Morin S. Chemical Force Titrations of Functionalized Si(111) Surfaces. Langmuir 2006;22:5301–5307. [PubMed: 16732656]

44. Landers, JP. Handbook of Capillary Electrophoresis. Landers, JP., editor. New York: CRC Press, Inc.; 1997. p. 894

45. Otevrel M, Kleparnik K. Electroosmotic Flow in Capillary Channels Filled with Nonconstant Viscosity Electrolytes: Exact Solution of the Navier-Stokes Equation. Electrophoresis 2002;23:3574–3582. [PubMed: 12412127]
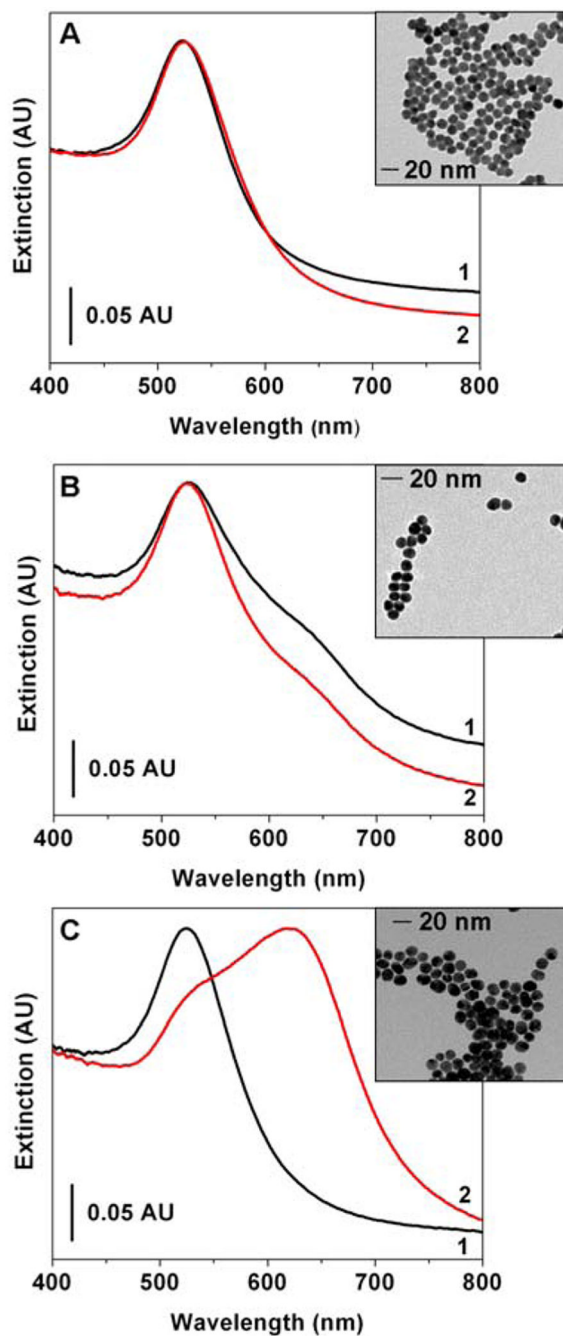
Figure 1. Characterization of gold nanoparticles using LSPR spectroscopy and TEM (inset)
(A) Au@citrate (d = 13.3 ± 0.6 nm) have an extinction maximum located at (1) 523.3 nm in water and (2) 524.8 nm in buffer. (B) Au@COOH (d = 10.9 ± 1.8 nm) have an extinction maximum located at (1) 521.5 nm in water and (2) 522.3 nm in buffer with a slight shoulder located ~625 nm in both spectra. (C) Au@NH$_2$ (d = 13.8 ± 2.0 nm) have an extinction maximum located at (1) 524.0 nm in water and (2) 617.5 nm with a shoulder at the original extinction maximum ~525 nm in buffer. In all buffer spectra, 10 mM tetraborate buffer (pH = 9.3) is used.
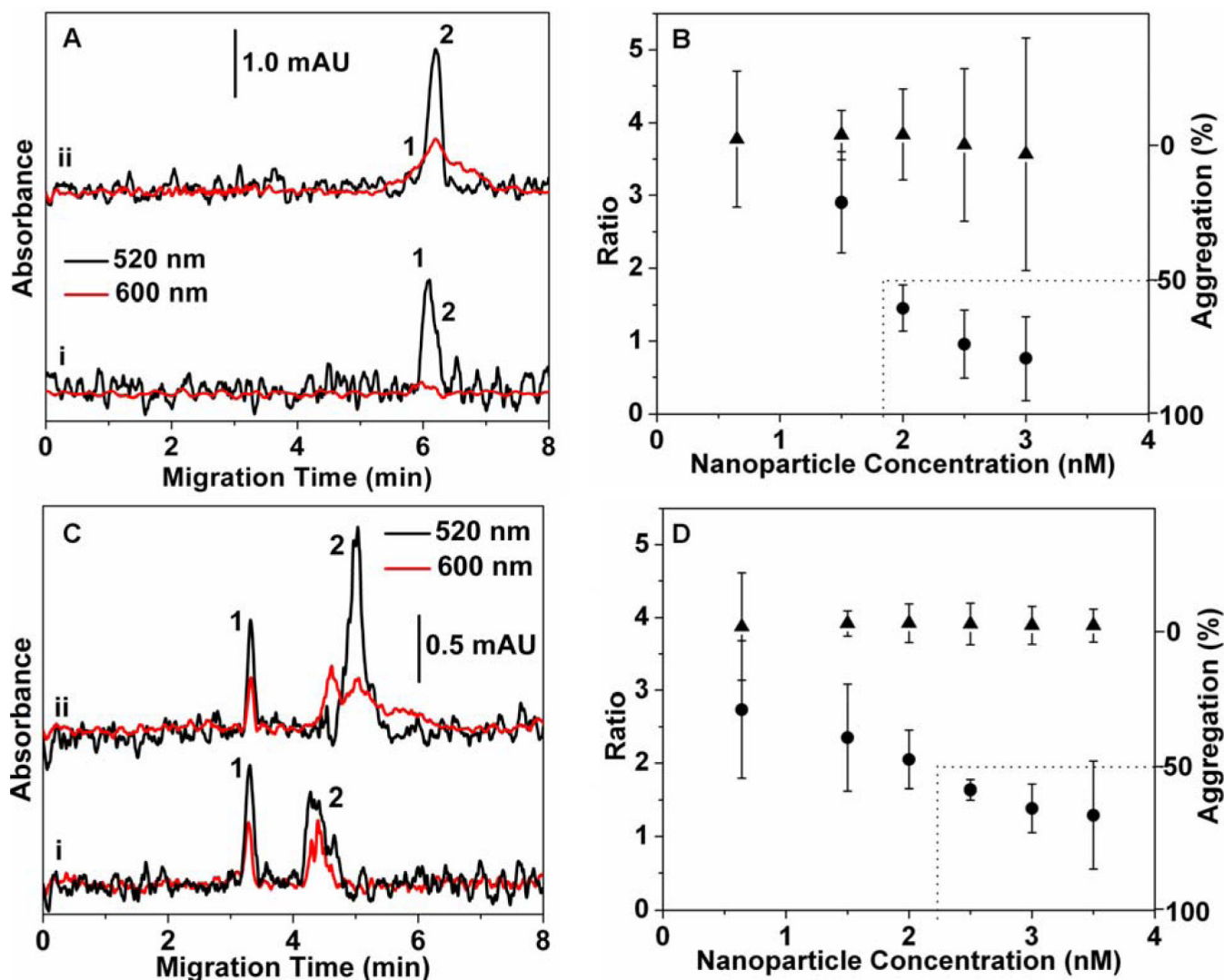
Figure 2. Dual-wavelength PDA detection of nanoparticles in a capillary
(A) Representative electropherograms for (i) 1.5 nM Au@COOH nanoparticles at λ_{det} = 520 nm (band 1 S/N = 12.4 and band 2 S/N = 6.8) and λ_{det} = 600 nm (band 1 S/N = 7.4 and band 2 S/N = 4.0). Representative electropherograms for (ii) 2.5 nM Au@COOH nanoparticles at λ_{det} = 520 nm (band 1 S/N = 3.0 and band 2 S/N = 19.4), and λ_{det} = 600 nm (band 1 S/N = 8.0 and band 2 S/N = 18.9). Determination of the CNC of Au@COOH nanoparticles. Triangle = Band 1 (t = 6.1 min) and Circle = Band 2 (t = 6.4 min). (C) Representative electropherograms for (i) 1.5 nM Au@NH$_2$ nanoparticles at λ_{det} = 520 nm (band 1 S/N = 16.1 and band 2 S/N = 11.1) and λ_{det} = 600 nm (band 1 S/N = 17.6 and band 2 S/N = 16.9). Representative electropherograms for (ii) 3.5 nM Au@NH$_2$ nanoparticles at λ_{det} = 520 nm (band 1 S/N = 12.0 and band 2 S/N = 21.0) and λ_{det} = 600 nm (band 1 S/N = 15.4 and band 2 S/N = 18.3). (D) Determination of the CNC of Au@NH$_2$ nanoparticles. Triangle = Band 1 (t = 3.3 min) and Circle = Band 2 (t = 4.4 min). In panels B and D, average areas for bands 1 and 2 were measured via integration techniques. Error bars represent propagated error from a minimum of three electropherograms.
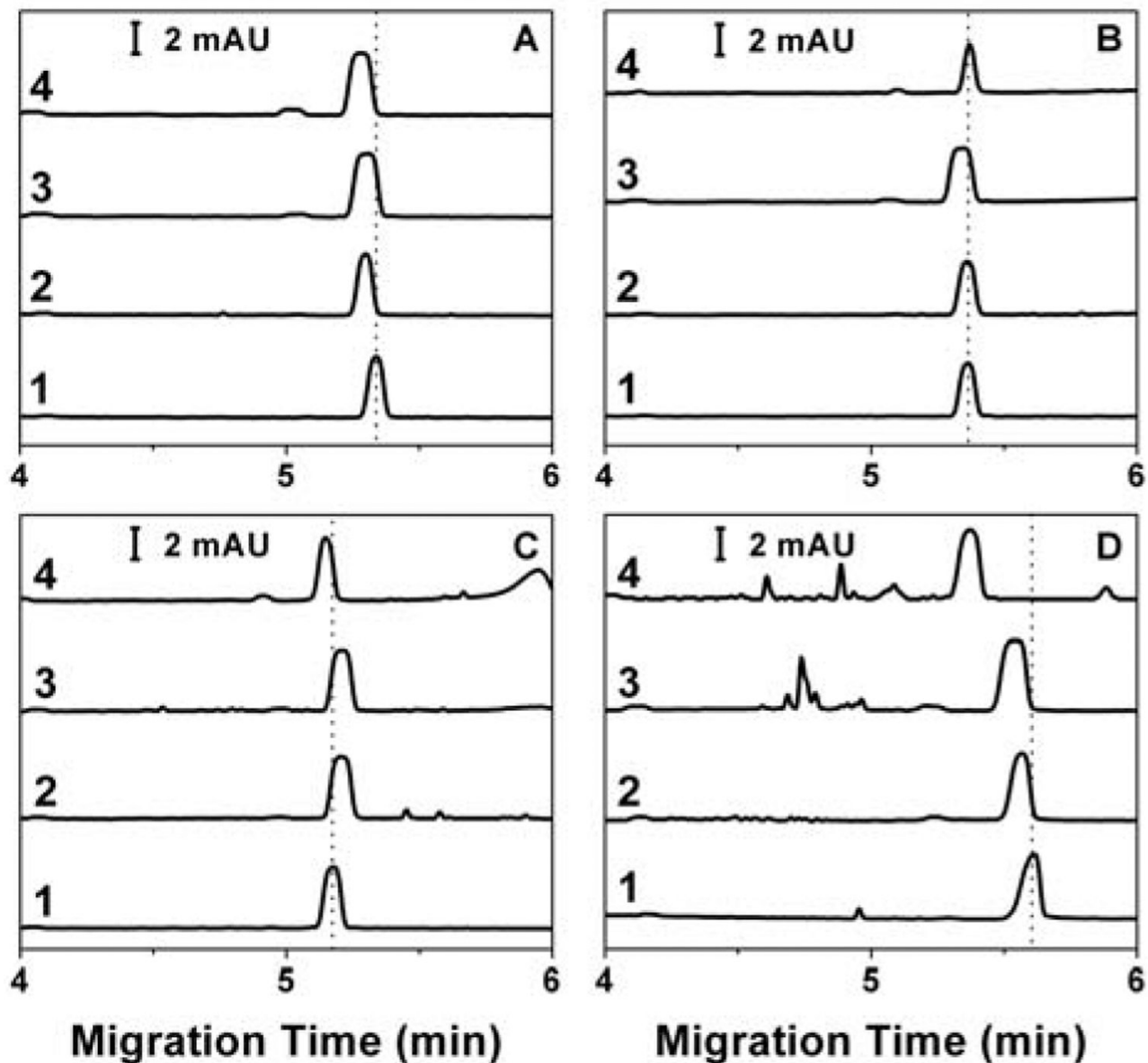
Figure 3. Evaluation of trends in the migration time of pyrocatechol as a function of nanoparticle concentration

Representative electropherograms in the presence of (A) silica, (B) Au@citrate, (C) Au@COOH, and (D) Au@NH$_2$ nanoparticles. In each case, nanoparticle bands are starred. 10 mM tetraborate buffer (pH = 9.3) is used and the "sample" injection order is nanoparticles (1 psi for 5 s), buffer (1 kV for 1 s), and neurotransmitters (10 kV for 10 s). Separation voltage = 20 kV, λ_{det} = 214 nm.

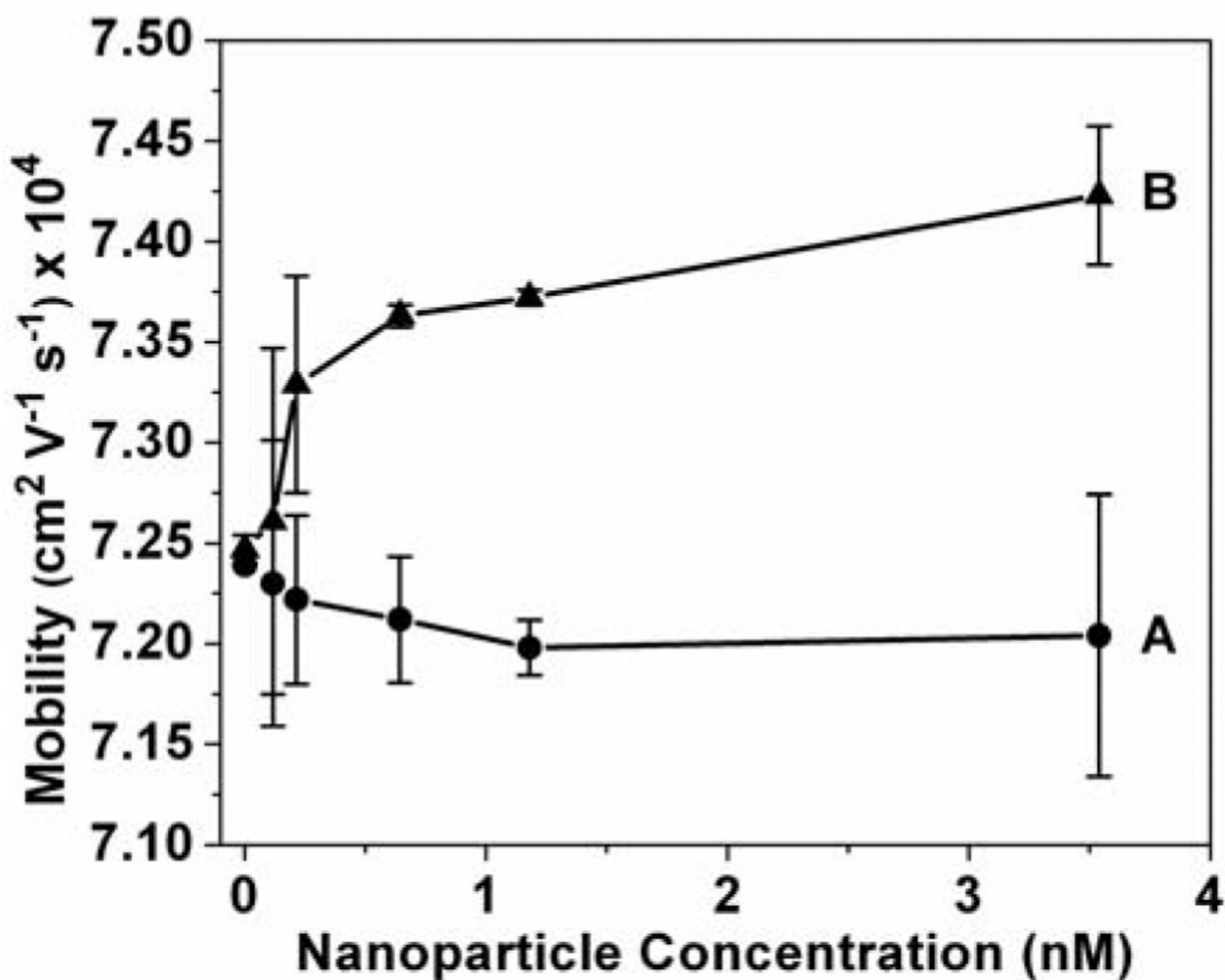**Figure 4. Comparison of dopamine mobility versus nanoparticle concentration**
Increasing concentrations (0 – 3.54 nM) of Au@COOH and Au@NH$_2$ nanoparticles have
opposite effects on dopamine mobility. (A) Increasing the concentration of Au@COOH
nanoparticles slightly decreases the mobility of dopamine. (B) Increasing the concentration of
Au@NH$_2$ nanoparticles increases the mobility of dopamine. Error bars represent the spread in
the data. If no error bars are visible, the error is included within the size of the data point itself.
The lines in the plot are included to guide the eye.
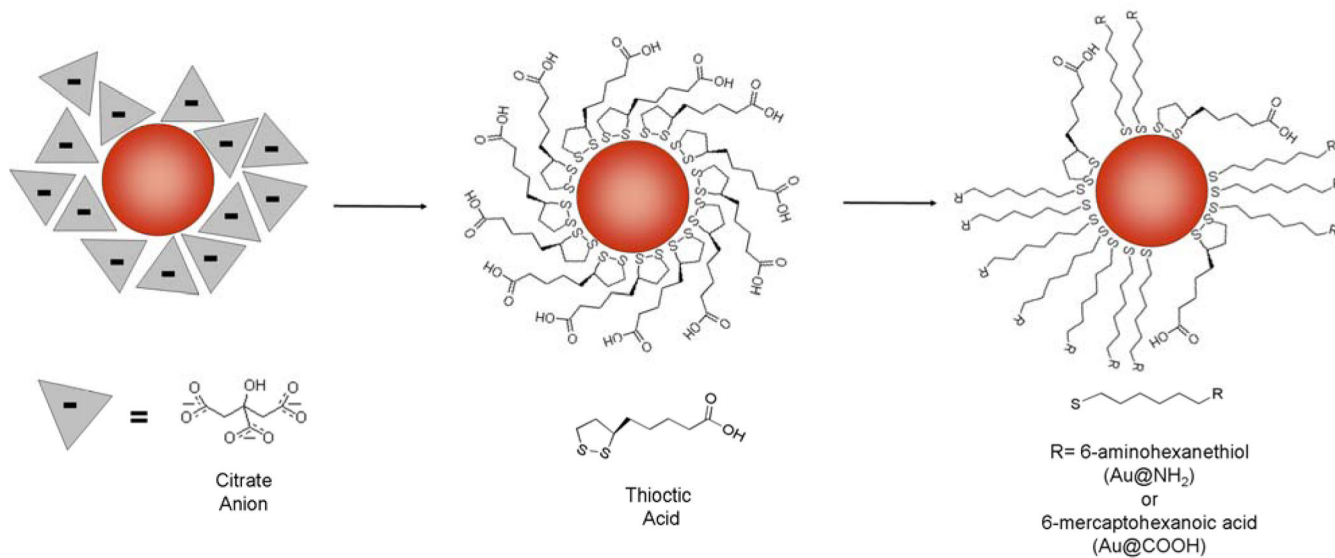
Scheme 1. Ligand exchange reaction on gold nanoparticles